



Cite this: *Nanoscale*, 2017, **9**, 10757

Amorphous boron nanorod as an anode material for lithium-ion batteries at room temperature†

Changjian Deng,^a Miu Lun Lau,^a Heather M. Barkholtz,^b Haiping Xu,^b Riley Parrish,^a Meiyue (Olivia) Xu,^b Tao Xu,^b Yuzi Liu,^c Hao Wang,^d Justin G. Connell,^e Kassiopsea A. Smith^a and Hui Xiong  ^{*a}

We report an amorphous boron nanorod anode material for lithium-ion batteries prepared through smelting non-toxic boron oxide in liquid lithium. Boron in theory can provide capacity as high as 3099 mA h g⁻¹ by alloying with Li to form B₄Li₅. However, experimental studies of the boron anode have been rarely reported for room temperature lithium-ion batteries. Among the reported studies the electrochemical activity and cycling performance of the bulk crystalline boron anode material are poor at room temperature. In this work, we utilized an amorphous nanostructured one-dimensional (1D) boron material aiming at improving the electrochemical reactivity between boron and lithium ions at room temperature. The amorphous boron nanorod anode exhibited, at room temperature, a reversible capacity of 170 mA h g⁻¹ at a current rate of 10 mA g⁻¹ between 0.01 and 2 V. The anode also demonstrated good rate capability and cycling stability. The lithium storage mechanism was investigated by both sweep voltammetry measurements and galvanostatic intermittent titration techniques (GITTs). The sweep voltammetric analysis suggested that the contributions from lithium ion diffusion into boron and the capacitive process to the overall lithium charge storage are 57% and 43%, respectively. The results from GITT indicated that the discharge capacity at higher potentials (>~0.2 V vs. Li/Li⁺) could be ascribed to a capacitive process and at lower potentials (<~0.2 V vs. Li/Li⁺) to diffusion-controlled alloying reactions. Solid state nuclear magnetic resonance (NMR) measurement further confirmed that the capacity is from electrochemical reactions between lithium ions and the amorphous boron nanorod. This work provides new insights into designing nanostructured boron materials for lithium-ion batteries.

Received 27th April 2017,
Accepted 20th June 2017

DOI: 10.1039/c7nr03017g

rsc.li/nanoscale

Introduction

Rechargeable lithium-ion batteries (LIB) with high energy density, high power density and long cycle life are in urgent need for the surging markets in portable electronics and electrical vehicles (EVs). Graphite is commercially used as an anode material owing to its good rate capability, low irrevers-

ible capacity, and good cycle life. However, the relatively low theoretical specific capacity (372 mA h g⁻¹) of graphite has limited its further implementation in applications such as EVs. As a result, extensive research efforts have been carried out to improve anode performance by developing new materials such as alloy anode materials, which are expected to exhibit much higher theoretical specific capacities (two- to ten-fold increase) compared to commercial graphite anodes.¹

Boron is an element of complexity. It exhibits the most varied polymorphisms of any of the elements: at least sixteen polymorphs have been reported to date² while the stable phase of boron is not yet established experimentally even under ambient conditions.³ Boron's complexities arise from the fact that it has only three valence electrons but they are sufficiently localized, which could shift between metallicity and insulating states by temperature, pressure and impurities.⁴⁻⁷ The electron deficient nature of boron could facilitate the inclusion of electrons while its common valence state (*i.e.*, trivalent boron) could allow the release of the extra electrons. Hence, this property of boron can be utilized for charging/discharging.

^aMicron School of Materials Science and Engineering, Boise State University, Boise, ID 83725, USA. E-mail: clairexiong@boisestate.edu

^bDepartment of Chemistry and Biochemistry, Northern Illinois University, DeKalb, IL 60115, USA

^cCenter for Nanoscale Materials, Argonne National Laboratory, Lemont, IL, 60439, USA

^dChemical Science and Engineering Division, Argonne National Laboratory, Lemont, IL, 60439, USA

^eJoint Center for Energy Storage Research, Argonne National Laboratory, Lemont, IL, 60439, USA

† Electronic supplementary information (ESI) available: Details of GITT techniques and the XPS survey scans of the as-prepared and 1st cycle samples. See DOI: 10.1039/c7nr03017g

Among the lithium–boron system, compounds such as B_3Li ,^{8,9} B_6Li_7 ¹⁰ and B_4Li_5 ^{11–13} have been reported, which in theory can provide 826, 2892 and 3099 mA h g⁻¹ in capacity, respectively. These compounds are generally composed of connected icosahedron B_{12} entities with Li residing between them.^{9,14} These systems are attractive for Li storage due to their high theoretical capacities and open structures for ion insertion. Although Li–B compound has been studied as an anode material for thermal batteries since 1990s,^{10,15} the reports on boron anode materials for room temperature LIB are scarce. From the limited reports, the electrochemical reactivity and the cycling performance of bulk crystalline boron with lithium are poor at room temperature.^{16–20} S. James investigated the Li–B alloy in $LiClO_4$ -propylene carbonate (PC) and stated that the Li–B alloy is a mixture of pure lithium and a Li–B compound with a stoichiometry in the vicinity of “ Li_7B_6 ” but no cycling performance of the electrode was reported.¹⁸ Sanchez and Belin *et al.* determined the electrochemical properties of the Li–B alloy in non-aqueous electrolytes.¹⁷ The LiB compound was found to have some discharge capacity but its capacity decayed rapidly within only a few cycles.¹⁷ Zhou *et al.* studied LiB compound¹⁹ in the electrolyte of 1 M anhydrous $LiPF_6$ in a 1:1 mixture of ethylene carbonate (EC) and dimethyl carbonate (DMC), which exhibited a first discharge capacity of 226 mA h g⁻¹ between 0 and 0.8 V *versus* Li/Li⁺. The discharge capacity decreased to 149 mA h g⁻¹ after 15 cycles. Recently, Ding *et al.* studied a new tetragonal boron (B_{50})²⁰ thin film with a thickness of 80 nm on a vanadium coated glass through a pulse laser deposition method. It was found that this thin film electrode exhibited only a capacity of 43 mA h g⁻¹ in a non-aqueous electrolyte at room temperature.²⁰ Based on the first-principles calculations, B_{50} is a metallic conductor and its very poor electrochemical activity at room temperature could be related to poor lithium ion diffusion (diffusion barrier is calculated as 2.59 eV) within the tetragonal B_{50} lattice. The charge storage capacity in the B_{50} film improves significantly at 85 °C, which is consistent with the first-principles simulations.

In this work, we developed an amorphous nanostructured one-dimensional (1D) boron material aiming at improving lithium ion diffusion in boron at room temperature. The structure of amorphous boron is closely related to that of commonly found crystalline β -rhombohedral boron which consists of a complex three-dimensional array of B_{12} icosahedral subunits, but with disorder occurring at the linking between these subunits.^{21,22} Research has shown that there could be lower volume strain during cycling in amorphous structures than that in the corresponding crystalline one, which results in the promoted electrochemical stability of amorphous structures.^{23,24} In addition, 1D nanostructured materials exhibit improved ion transport along the z axial direction, which leads to enhanced electrochemical performance.^{25–27} Moreover, nanostructured materials can offer several advantages over their bulk counterparts: shorter diffusion length for both Li ions and electron transport; a larger surface contact area enhancing the kinetics at the electrode/electrolyte interface;

better strain relaxation and volume accommodation, which lead to enhanced stability.

Herein, we tested an amorphous boron nanorod anode for LIBs at room temperature, which exhibits a reversible capacity of 170 mA h g⁻¹ at 10 mA g⁻¹ for 25 cycles. The unique amorphous nanostructure enhances the currently reported capacity of 43 mA h g⁻¹ of the crystalline boron anode by ~400% at room temperature.²⁰ It also demonstrates a good rate capability and promising cycling performance, delivering up to 100 mA h g⁻¹ reversible capacity after 500 cycles at a rate of 0.5C (*n*C rate: discharge in 1/*n* hours). Structural characterization by transition electron microscopy (TEM) and X-ray diffraction (XRD) reveals that the as-prepared boron nanorod electrode is amorphous. It is postulated through the galvanostatic intermittent titration technique (GITT) measurement that the capacity at higher potential (>~0.2 V *vs.* Li/Li⁺) can be attributed to the surface capacitive process and that at lower potential (<~0.2 V *vs.* Li/Li⁺) is due to the solid state Li ion diffusion within B. To understand the contribution from each process, sweep voltammetry measurements were conducted and it was estimated that capacities resulting from diffusion control and from the capacitive process are 57% and 43%, respectively. Solid state NMR further confirmed that lithium ions are actively involved in the electrochemical reaction with boron.

Experimental

Synthesis of amorphous boron nanorod

The amorphous boron nanorod materials were synthesized by our top down process reported previously.²⁸ 500 mg of B_2O_3 was dried at 110 °C under vacuum and then was thoroughly ground in the glove box. Subsequently, B_2O_3 powders were added into molten Li with a molar ratio of B_2O_3 :Li = 1:6 at 200 °C under sonication. Afterwards, the temperature was increased to 250 °C and maintained for 2 hours. After the reaction was complete, the product was cooled down and taken out of the glove box. In order to obtain the pure boron nanorod sample, the samples were first washed with methanol to remove unreacted lithium and then washed thoroughly with hot water, dilute potassium hydroxide solution, dilute hydrochloric acid solution and cold water to remove the Li, Li_2O , LiB_2 , LiB_4 and B_2O_3 residues.

Characterization

The XRD pattern was obtained by using a Rigaku Miniflex diffractometer with Cu K α irradiation at $\lambda = 1.5406$ Å. The morphology and microstructures were examined by field emission scanning electron microscopy (FE-SEM, JEOL JSM-7500F field emission) and TEM (FEI Titan 80-300 ST). XPS was conducted by using a Specs PHOIBOS 150 hemispherical energy analyzer using a monochromated Al K α X-ray source. Survey spectra were collected using a pass energy of 40 eV, and spectra were referenced to the binding energy of graphite at 284.0 eV. XPS samples were loaded without air exposure through an Ar glove box connected directly to the UHV system. Solid state ⁷Li NMR

measurement was performed with a Bruker Avance III spectrometer operating at a magnetic field strength of 7.04 T. A pulse delay of 10 s was used, and a total of 256 scans were acquired for each spectrum. The samples were spinning at 60 kHz at 283 K. The Energy Dispersive X-Ray Spectroscopy (EDS) study of boron nanorods and the raw boron oxide powder was conducted in a Tescan-Vega SEM equipped with an Oxford INCAx-act Analytical Standard EDS detector.

Electrochemical measurement

Electrochemical characterization was conducted using a half-cell against a Li counter electrode. The boron electrodes were prepared by mixing of 70% boron active material, 10% graphite (Fisher Chemical), 10% super carbon C65 (Timcal America Inc.) and 10% sodium carboxymethyl cellulose (CMC, Dow Chemical Company) and casting the slurry on a copper current collector. After overnight vacuum baking at 70 °C, the electrode was punched into 1.5 cm dia. discs using a Precision Disc Cutter (MTI) with a loading density of 0.6–0.8 mg cm⁻². Coin cells were prepared with the boron electrode, Celgard 2325 separator, lithium (FMC) counter electrode in 1.2 M lithium hexafluorophosphate (LiPF₆) in ethyl carbonate (EC) and ethylmethyl carbonate (EMC) (3 : 7 w/w) in an argon filled dry glove box (O₂ < 0.5 ppm). The coin cells were tested at 10 mA g⁻¹ with a potential window of 0.01 to 2 V in an Arbin battery tester. A cell of three-electrode configurations was tested for CV with a potential window of 0.01 to 2 V at varying scan rates of 0.1–10 mV s⁻¹. CVs were conducted for at least three scans at each scan rate. GITT was conducted in a three-electrode cell with a potential window of 0.01 to 2 V at the rate of 10 mA g⁻¹. The cell was first cycled for 8 cycles and then discharged at 10 mA g⁻¹ for a pulse of 30 min followed by a relaxation of 2 h to approach the steady state value. The process was repeated to the fully discharged state of 0.01 V.

Results and discussion

Our previous work²⁸ shows that nanoscale rod-like boron can be synthesized by simply smelting boron oxide powders in molten lithium under sonication. Hereby, we continue to utilize this method to synthesize boron nanorods and investigate their nanoscale electrochemical interactions between these boron nanorods and lithium ions. The preparation of boron nano-rod materials can be found in our previous report.²⁸ In brief, the mixture of boron nanorods, Li, LiB_x, Li₂O and B₂O₃ was obtained after the reaction of B₂O₃ powders with molten Li under sonication. The mixture was then purified using alcohol, water, and diluted basic and acidic solutions in a sequence to obtain pure amorphous boron nanorods.

The structure of boron materials was examined by XRD, as shown in Fig. 1(a). Only a broad band with weak intensity was observed, which indicates the amorphous feature of the as-prepared sample. The crystallographic and morphological properties were determined by TEM. The 1D nano-rod structure with ~250 nm diameter is shown in Fig. 1(b). Moreover, the

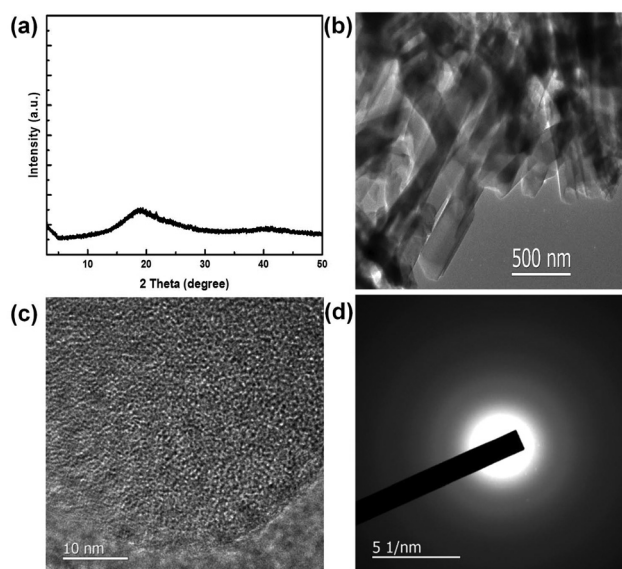


Fig. 1 (a) XRD pattern, (b) TEM image, (c) high resolution TEM image and (d) selected area electron diffraction (SAED) pattern of the as prepared nano-rod boron materials.

distribution of the nanorod diameter is quite narrow, in agreement with the previous study.²⁶ Both the featureless image shown in Fig. 1(c) and the characteristic diffusive ring in the SAED pattern shown in Fig. 1(d) suggest that the as-prepared 1D boron nanorod is amorphous, which corroborates well with the XRD results.

The EDS study of the as-prepared sample and the raw boron oxide powder shows that the nanorods are made of pure elemental boron (ESI, Fig. S1†). Fig. 2(a) and (b) show the as-prepared powders and cycled boron electrodes, respectively. Both samples exhibit a smooth surface with a uniform diameter of ~250 nm and a length of ~1 μm, which suggests that the 1D boron nanorod maintains its morphology after cycling. The preferential elongated nano-rod morphology instead of a nanosphere is due to the presence of sonication during the reaction of lithium with B₂O₃.^{28,29} The stream of ultrasonic propagation transfers momentum in the molten lithium solution, leading to a linear lithiation in B₂O₃ powders. Since the momentum distribution is not uniform in the lithium solution, the length of the nano-rods varies with momentum during lithiation.

The electrochemical performance of the amorphous boron nanorod anode was investigated using coin-type half cells with Li as the counter electrode. All of the coin cells were tested at room temperature. Fig. 3(a) shows the galvanostatic charge and discharge voltage profiles of the amorphous boron nanorod electrode at a current rate of 10 mA g⁻¹ cycled between 0.01 and 2.0 V. The 1st cycle discharge and charge capacity are 419.10 and 205.16 mA h g⁻¹, respectively, corresponding to a Coulombic efficiency of 48.95%. The irreversible capacity loss might result from the formation of a solid electrolyte interphase (SEI) between the electrode and the electrolyte, which commonly occurs in an alloy anode.³⁰ After eight cycles, the electrode exhibits a reversible capacity of ~170 mA g⁻¹,

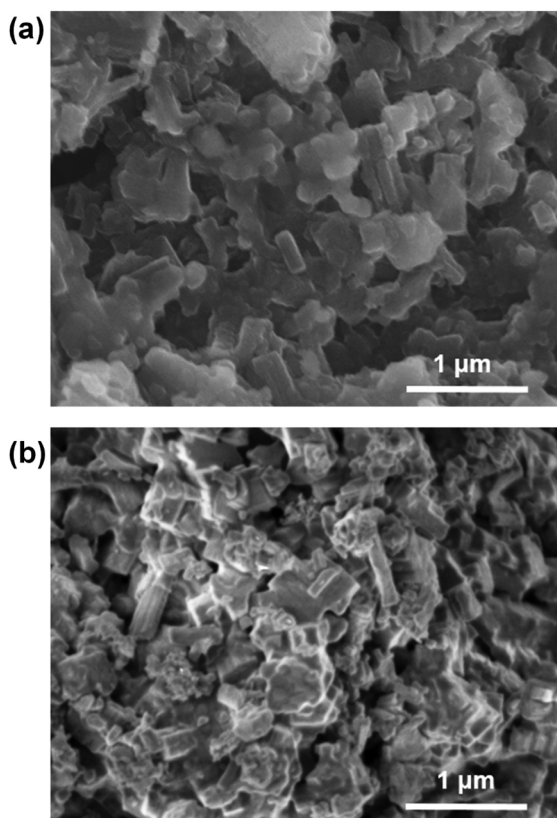


Fig. 2 FE-SEM images of (a) the as-prepared and (b) cycled nano-rod boron sample.

corresponding to a LiB_{15} compound, with a Coulombic efficiency of 97.7%. This reversible capacity is much higher than the previous report on a crystalline B_{50} thin film (44 mA h g^{-1}) at room temperature,²⁰ which can be attributed to the improved lithium diffusion in the 1D nanostructure and amorphous structure.²⁵ There are a few plateaus appearing in the charge/discharge curves at low voltages, indicating two phase regions of the possible Li_xB alloy. The peaks shown in the differential capacity (dQ/dV) plots in Fig. 3(b) correspond to the plateaus observed in the charge/discharge curves (Fig. 3(a)). During the first discharge, one irreversible peak at 1.0 V and three peaks at lower voltages (0.192 V, 0.106 V, and 0.069 V) were clearly observed. During charging, three corresponding oxidation peaks located at 0.237 V, 0.149 V and 0.107 V, respectively, are observed. The irreversible peak at 1 V is attributed to the side reaction between the electrode and the electrolyte and the formation of the SEI layer. The three redox peaks appearing here at lower voltages in dQ/dV plots are not seen in the B_{50} thin film reported previously,²⁰ which explains why the amorphous boron nanorod electrode has a much higher capacity due to enhanced electrochemical reactivity between lithium and amorphous nanostructured boron. There are no additional peaks and no significant peak shift in all the observed peaks in the subsequent cycling, indicating that the phase transitions are reversible.

Since one of the potential benefits of amorphous materials is the enhanced kinetics and electrochemical stability,^{23,24} we conducted experiments on the amorphous boron nanorod

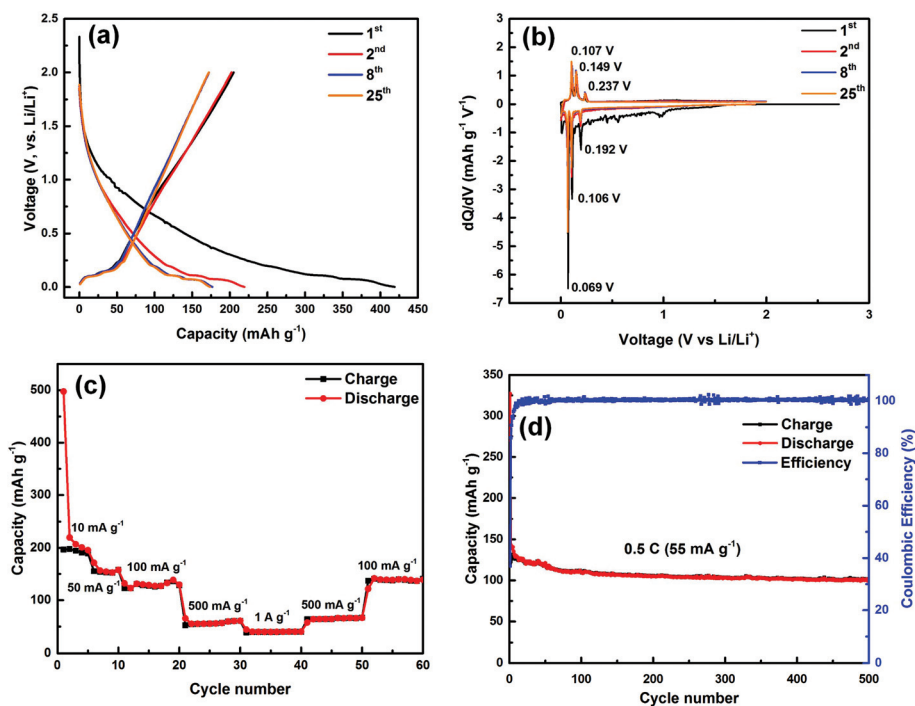


Fig. 3 Electrochemical characterization and electrode performance of the amorphous boron nanorod anode: (a) charge/discharge profile, (b) differential capacity versus voltage (dQ/dV) of the electrode cycled at 10 mA g^{-1} , (c) rate capability, and (d) cycling performance of the electrode with a current rate of 55 mA g^{-1} . All of the above cycling performances are with the potential window of 0.01–2 V vs. Li/Li^+ at room temperature.

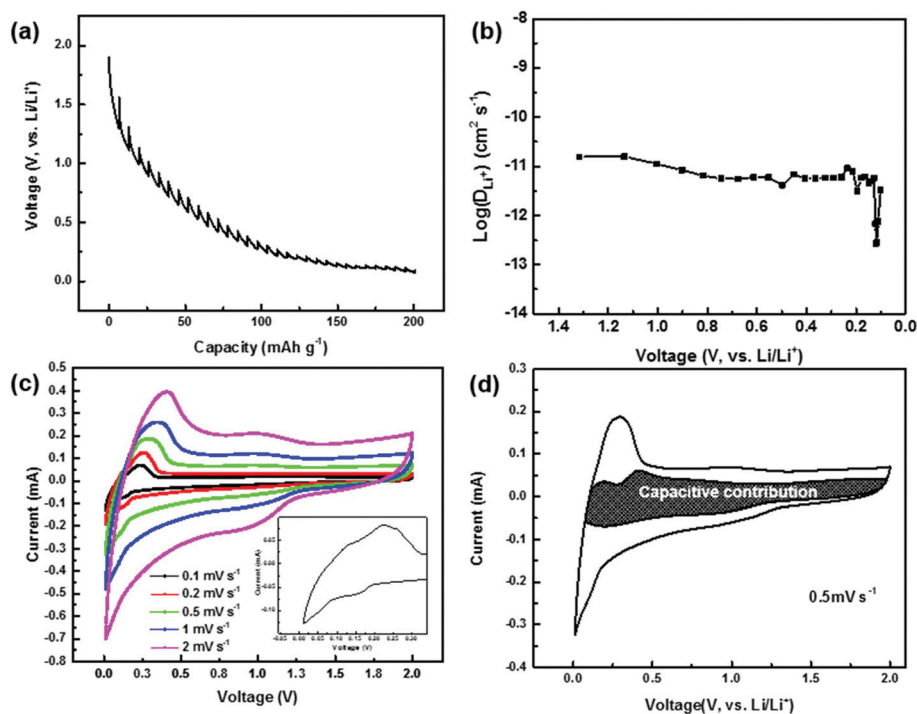


Fig. 4 (a) GITT profile. (b) Diffusivity as a function of states of charge. (c) Cyclic voltammograms between 0.01 and 2 V with scan rates of 0.1, 0.2, 0.5, 1 and 2 mV s^{-1} (inset: low-potential region with the scan rate of 0.1 mV s^{-1}). (d) Capacitive contribution in the amorphous boron nanorod electrode at the scan rate of 0.5 mV s^{-1} .

electrode for rate capability (Fig. 3c) and cycling performance (Fig. 3d) at a rate of 5 mA g^{-1} (0.5C). The amorphous boron nanorod electrode exhibits great rate capability at different cycling rates varying from 10 to 1000 mA g^{-1} as shown in Fig. 3(c). It delivered specific discharge capacities of 195.6, 157.8, 129.7, 60.9, and 40.3 mA h g^{-1} at current rates of 10, 50, 100, 500, and 1000 mA g^{-1} , respectively. The capacity moderately decreased with the increase of current density. At the highest current rate of 1 A g^{-1} the discharge capacity approached 40.6 mA h g^{-1} . When the current rates were ramped back to 500 and 100 mA g^{-1} after a variety of cycling rates, its capacity returned to ~ 64 and ~ 136 mA h g^{-1} , respectively, suggesting good capacity retention and rate capability. In the cycling performance study shown in Fig. 3(d), after 500 cycles, the electrode maintained a reversible capacity of 102 mA h g^{-1} with a capacity retention rate of 83.47%.

GITT measurement (Fig. 4(a)) was performed to understand the kinetic properties of the amorphous boron nanorod electrode, particularly Li diffusion coefficient during the electrochemical interaction between lithium and boron (the details of GITT analysis can be found in the ESI†). The log plot of the Li diffusivity as a function of voltage is shown in Fig. 4(b). It demonstrates that the diffusion associated with the sloping region ($> \sim 0.2$ V vs. Li/Li^+) is quite stable and is much faster than that of the plateau region ($< \sim 0.2$ V). The diffusion coefficient dramatically drops when the voltage is below 0.2 V, where phase transitions occur as indicated by the dQ/dV plots shown in Fig. 3(b). The diffusion in the sloping region is about

2-order of magnitude larger than that of the plateau regions. This indicates that at the sloping region there are more accessible surface adsorption sites for lithium ion diffusion. At the plateau region ($< \sim 0.2$ V) where lithium and boron form alloys, diffusion of the lithium ion is poor as it has to overcome higher energy barriers to travel between B_{12} icosahedra. Since the capacity contributed from the sloping region is much larger than that from the plateau regions, the capacitive process plays a more significant role than that of the alloying reactions in lithium storage mechanism in this material. And the sluggish diffusion in alloying reactions might explain the lower capacity compared with the theoretical one.

In order to investigate the charge storage kinetics of the amorphous boron nanorod electrode, cyclic voltammograms (CVs) between 0.01 and 2 V with various scan rates of 0.1, 0.2, 0.5, 1.0 and 2.0 mV s^{-1} were performed (Fig. 4c). A low-potential region with a scan rate of 0.1 mV s^{-1} is highlighted in Fig. 4c inset, where three cathodic peaks at 0.16, 0.06 and 0.01 V and three corresponding anodic peaks at 0.26, 0.22 and 0.13 V can be resolved, in agreement with the dQ/dV plots shown in Fig. 3(b). The sweep voltammetry also provides insights in terms of diffusion and capacitive contribution of the Li storage mechanism, which can be characterized by analyzing the data at various sweep rates according to the equation³¹

$$i = av^b \quad (1)$$

Where measured current i obeys a power law relationship with a scan rate. Both a and b in the equation are adjustable

parameters. A b value of 1 indicates that the charge storage is controlled by a capacitor-like kinetics, which is one of the characteristic features of capacitive contribution.³² A $b = 0.5$ indicates that the charge storage process is limited by diffusion.³³ At potentials higher than ~ 0.2 V, the b -values are in the range of 0.73–0.75. At potentials smaller than ~ 0.2 V, the b -values are ~ 0.58 , indicating that the charge storage mostly comes from the Li ion alloying reactions. Since the capacitive contribution is involved in the process, we estimated that the surface area normalized capacitance is larger than that of a typical double layer capacitor, $10\text{--}50 \mu\text{F cm}^{-2}$,³⁴ indicating the lithium storage mechanism on the surface is dominated by pseudocapacitive contribution.

In addition, the diffusion and capacitive contribution to the current response at the fixed potential can be quantitatively examined by the following equation:³²

$$i(V) = k_1\nu + k_2\nu^{1/2} \quad (2)$$

where the term $k_1\nu$ and $k_2\nu^{1/2}$ represent the contributions from surface capacitive and diffusion controlled process, respectively. Therefore, by determining both k_1 and k_2 , we are able to quantitatively estimate the fraction of current contributed by the capacitor-like process and the diffusion-limited process. The voltammetric response for the amorphous boron nanorod electrode at a slow scan rate of 0.5 mV s^{-1} in Fig. 4(d) demonstrates that the contribution of capacitor-like charge storage (shaded area) is quite significant, consistent with the electrochemical results discussed above. The diffusion-controlled contribution is largely occurring at the peak region at lower potentials, corresponding to the alloy reaction and is in agreement with the voltage profile (Fig. 3a) and GITT results (Fig. 4b). The capacitive process contributed $\sim 43\%$ of the total lithium charge storage, which is slightly smaller than that from the diffusion-controlled process related to Li alloying reactions (57%). This result indicates that increasing accessible surface sites for possible lithium ion adsorption through nanostructured boron compared to thin film boron could enhance the charge storage capacity.

To understand the chemical environment change of the amorphous boron nanorod electrode during cycling, *ex situ* XPS was performed with the as-prepared and 1st discharged (lithiated) samples (ESI, Fig. S4†). Quantification of the surface speciation revealed that the atomic percentage of F increased with cycling, from 5% in the as-prepared sample to 22% in the 1st discharged sample, suggesting the growth of an SEI on the surface. Indeed, LiF is a common compound found in the SEI layer at alloy-type anodes.^{30,35} Although XPS analysis did not clearly show redox of the boron species, it is possible that surface reactions during sample transfer obscure lithiation in the bulk of the sample, which is not detected by the highly surface-sensitive XPS measurement. As a result, solid state ^7Li NMR was also performed to understand the chemical environment evolution in the bulk of the amorphous boron nanorod electrode upon cycling (Fig. 5). The ^7Li NMR spectra of the discharged (lithiated) and charged (delithiated) samples were nor-

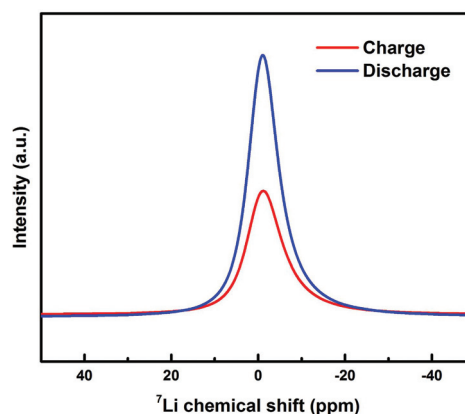


Fig. 5 Solid state ^7Li NMR spectroscopy of a charged and a discharged amorphous boron nanorod sample.

malized to the sample mass. One resonance was observed at around -1.0 ppm. The resonance of the charged sample suggests the retention of lithium from the previous cycling (potentially caused by the lithium ion trapping during the electrochemical process). It is noticed that the line width of the NMR spectra between the charged and discharged samples differ and this difference may be caused by the change in chemical environment. The similarity between the chemical shifts of these two spectra indicates that the lithium moves between two similar chemical environments.

Conclusions

Amorphous nanostructured 1D boron material was successfully prepared by the top-down process as an anode for lithium ion batteries. At room temperature, it delivered 170 mA h g^{-1} reversible capacity at the rate of 10 mA g^{-1} between 0.01 and 2 V, which is four-fold larger than that from a previous study of the crystalline boron thin film.²⁰ The electrode also exhibited promising rate capability, as well as cycling performance. It shows a reversible capacity of 100 mA h g^{-1} after 500 cycles at the rate of 0.5C. GITT measurement indicated that lithium diffusion due to surface adsorption at higher potential ($> \sim 0.2$ V vs. Li/Li^+) is significantly higher than that from alloying reactions at lower potentials ($< \sim 0.2$ V vs. Li/Li^+), which can be ascribed to the nanostructure effect. Sweep voltammetric analysis suggested that the contribution of pseudocapacitance to the lithium storage is larger than that from lithium diffusion in the alloying reactions. Our results indicate that the sluggish kinetics of lithium–boron alloying reactions impede the electrode from achieving its high theoretical capacity. Our work provides insights into material design for new boron-related electrode materials such as borophene. We believe that tailoring the nanostructure as well as the surface chemistry of the boron electrode are critical to enhance its electrochemical reactivity at room temperature for lithium-ion batteries.

Studies on the improvement of electrode kinetics are currently underway and could significantly improve the electrochemical performance of boron materials, therefore providing a new class of anode materials for lithium-ion batteries.

Author contributions

H. Xiong designed all experiments. T. Xu designed the synthesis of the material. C. Deng, M. L. Lau, and R. Parrish prepared the electrodes. C. Deng, M. L. Lau, and R. Parrish conducted electrochemical measurements. C. Deng and H. Xiong analyzed the data. H. M. Barkholtz, H. Xu, and M. Xu prepared the boron materials. M. Xu is a volunteer high school student from Christian Life School in Kenosha, WI, USA. Y. Liu and K. Smith conducted electron microscopic characterization. H. Wang collected and analyzed the solid ^7Li NMR data. J. Connell collected and analyzed the XPS data. All authors discussed the results and contributed to the manuscript preparation. C. Deng and H. Xiong wrote the manuscript.

Acknowledgements

H. Xiong gratefully acknowledges discussions with Dr T. Rajh. T. Xu acknowledges the financial support from the National Science Foundation (CBET-1150617). The use of the Center for Nanoscale Materials was supported by the U. S. Department of Energy, Office of Science, Office of Basic Energy Sciences, under Contract No. DE-AC02-06CH11357.

References

- 1 M. N. Obrovac and V. L. Chevrier, *Chem. Rev.*, 2014, **114**, 11444–11502.
- 2 J. Donohue, *Structures of the elements*, John Wiley and Sons, Inc, United States, 1974.
- 3 *Journal of Physical and Chemical Reference Data*, ed. M. W. Chase Jr., American Chemical Society and American Institute of Physics for the National Institute of Standards and Technology, USA, 4th edn, 1998, Monograph 9.
- 4 A. R. Oganov, J. H. Chen, C. Gatti, Y. Z. Ma, Y. M. Ma, C. W. Glass, Z. X. Liu, T. Yu, O. O. Kurakevych and V. L. Solozhenko, *Nature*, 2009, **457**, 863–867.
- 5 T. Lundstrom, *J. Solid State Chem.*, 1997, **133**, 88–92.
- 6 R. J. Nelmes, J. S. Loveday, D. R. Allan, J. M. Besson, G. Hamel, P. Grima and S. Hull, *Phys. Rev. B: Condens. Matter*, 1993, **47**, 7668–7673.
- 7 E. Y. Zarechnaya, L. Dubrovinsky, N. Dubrovinskaia, Y. Filinchuk, D. Chernyshov, V. Dmitriev, N. Miyajima, A. El Goresy, H. F. Braun, S. Van Smaalen, I. Kantor, A. Kantor, V. Prakapenka, M. Hanfland, A. S. Mikhaylushkin, I. A. Abrikosov and S. I. Simak, *Phys. Rev. Lett.*, 2009, **102**, 185501.
- 8 G. Mair, H. G. von Schnering, M. Worle and R. Nesper, *Z. Anorg. Allg. Chem.*, 1999, **625**, 1207–1211.
- 9 H. B. Borgstedt and C. Guminski, *J. Phase Equilib.*, 2003, **24**, 572–574.
- 10 S. Dallek, D. W. Ernst and B. F. Larrick, *J. Electrochem. Soc.*, 1979, **126**, 866–870.
- 11 M. Worle and R. Nesper, *Angew. Chem., Int. Ed.*, 2000, **39**, 2349–2353.
- 12 J. R. Letelier, Y. N. Chiu and F. E. Wang, *J. Less-Common Met.*, 1979, **67**, 179–184.
- 13 F. E. Wang, *Metall. Trans. A*, 1979, **10**, 343–348.
- 14 B. Albert, *Eur. J. Inorg. Chem.*, 2000, 1679–1685.
- 15 P. Sanchez, C. Belin, G. Crepy and A. Deguibert, *J. Mater. Sci.*, 1992, **27**, 240–246.
- 16 A. Netz, R. A. Huggins and W. Weppner, *Ionics*, 2001, **7**, 433–439.
- 17 P. Sanchez, C. Belin, C. Crepy and A. Deguibert, *J. Appl. Electrochem.*, 1989, **19**, 421–428.
- 18 S. D. James, *J. Appl. Electrochem.*, 1982, **12**, 317–321.
- 19 D. B. Zhou, Z. J. Liu, X. K. Lv, G. S. Zhou and J. Yin, *Electrochim. Acta*, 2006, **51**, 5731–5737.
- 20 X. L. Ding, X. Lu, Z. Fu and H. Li, *Electrochim. Acta*, 2013, **87**, 230–235.
- 21 R. G. Delaplane, U. Dahlborg, W. S. Howells and T. Lundstrom, *J. Non-Cryst. Solids*, 1988, **106**, 66–69.
- 22 R. G. Delaplane, U. Dahlborg, B. Graneli, P. Fischer and T. Lundstrom, *J. Non-Cryst. Solids*, 1988, **104**, 249–252.
- 23 L. Y. Beaulieu, K. C. Hewitt, R. L. Turner, A. Bonakdarpour, A. A. Abdo, L. Christensen, K. W. Eberman, L. J. Krause and J. R. Dahn, *J. Electrochem. Soc.*, 2003, **150**, A149–A156.
- 24 T. D. Hatchard, M. N. Obrovac and J. R. Dahn, *J. Electrochem. Soc.*, 2006, **153**, A282–A287.
- 25 B. Wang, B. Luo, X. L. Li and L. J. Zhi, *Mater. Today*, 2012, **15**, 544–552.
- 26 H. Pang, X. Li, Q. Zhao, H. Xue, W.-Y. Lai, Z. Hu and W. Huang, *Nano Energy*, 2017, **35**, 138–145.
- 27 B. Li, P. Gu, Y. Feng, G. Zhang, K. Huang, H. Xue and H. Pang, *Adv. Funct. Mater.*, 2017, **27**, 1605784.
- 28 A. Chakrabarti, T. Xu, L. K. Paulson, K. J. Krise, J. A. Maguire and N. S. Hosmane, *J. Nanomater.*, 2010, 589372.
- 29 P. Marmottant and S. Hilgenfeldt, *Nature*, 2003, **423**, 153–156.
- 30 E. Peled, D. Golodnitsky, C. Menachem and D. Bar-Tow, *J. Electrochem. Soc.*, 1998, **145**, 3482–3486.
- 31 H. Lindstrom, S. Sodergren, A. Solbrand, H. Rensmo, J. Hjelm, A. Hagfeldt and S. E. Lindquist, *J. Phys. Chem. B*, 1997, **101**, 7717–7722.
- 32 J. Wang, J. Polleux, J. Lim and B. Dunn, *J. Phys. Chem. C*, 2007, **111**, 14925–14931.
- 33 A. J. Bard and L. R. Faulkner, *Electrochemical Methods: Fundamentals and Applications*, John Wiley & Sons, New York, 1980.
- 34 B. E. Conway, V. Birss and J. Wojtowicz, *J. Power Sources*, 1997, **66**, 1–14.
- 35 A. M. Andersson and K. Edstrom, *J. Electrochem. Soc.*, 2001, **148**, A1100–A1109.